NANO · MICRO small
www.small-journal.com

Hierarchically Interpenetrated and Reentrant Microcellular Frameworks for Stretchable Lithium Metal Batteries

Yoojoo An, Nayeon Kim, Soo Yeong Hong, Arum Jung, Eunji Kim, Yonghee Lee, Jinhan Cho, Bongjun Yeom, and Jeong Gon Son**

With the rapid development of human-friendly wearable devices, energy storage components are required to have skin-like stretchability or free-form to fit closer and more comfortably to the human body. This study introduces a hierarchically interpenetrated reentrant microcellular structure combined with 2D cellular graphene/MXene/carbon nanotubes (CNTs) and 3D cellular melamine foam. This composite structure works as a stretchable framework of lithium metal composite electrodes to provide stretchability for lithium metal electrodes, which are promising as next-generation energy storage systems. The interpenetrated but independent cellular structures successfully obtain stable structural deformability from the nonconductive and deformable melamine foam, while at the same time, high electrical conductivity, lithiophilicity, and mechanical stability of the graphene/CNT/MXene network serve as a lithium deposition support during the electrodeposition of lithium. The reentrant structure is fabricated by radial compressing the hierarchical cellular structures to take advantage of the structural stretchability of the accordion-like reentrant frameworks. The lithium-deposited composite electrodes exhibit much lower overpotential during Li stripping and plating than lithium metal foil anodes and show stable electrochemical performances under 30% of mechanical strain. The reentrant microcellular electrodes offer great potential for advanced designs of lithium metal electrodes for stretchable batteries with high energy density.

1. Introduction

Recently, wearable electronic devices are getting closer to humans, appealing attention for their potential applications in smart clothing, electronic skin, healthcare devices attached to the body or implantable devices inserted into the body, bendable/stretchable smartphones, etc.[1–5] Accordingly, energy storage systems of wearable devices should also be stretchable or deformable to have mechanical properties close to those of the human body,[6–8] while simultaneously satisfying high energy storage performance in a small volume. However, most of the batteries developed so far stay in a rigid form which does not conform to the shape of the bendable/stretchable electronics. The reasons are that most of the active materials of the electrodes responsible for energy storage are hard inorganic particles, and in addition to electrode materials, various components, including current collectors, separators, electrolytes, and encapsulation, constitute the energy storage device, so the providing stretchability of all of them should be considered.

Y. An, J. Cho, J. G. Son
KU-KIST Graduate School of Converging Science and Technology
Korea University
Seoul 02841, Republic of Korea
E-mail: jgson@kist.re.kr

Y. An, N. Kim, S. Y. Hong, J. Cho, J. G. Son
Soft Hybrid Materials Research Center
Korea Institute of Science and Technology
Seoul 02792, Republic of Korea

N. Kim, A. Jung, B. Yeom
Department of Chemical Engineering
Hanyang University
Seongdong-gu, Seoul 04763, Republic of Korea
E-mail: byeom@hanyang.ac.kr

E. Kim, Y. Lee
National Nano Fab Center (NNFC)
Daejeon 34141, Republic of Korea

J. Cho
Department of Chemical and Biological Engineering
Korea University
Seoul 02841, Republic of Korea

E. Kim
Department of Chemical and Biomolecular Engineering
Korea Advanced Institute of Science and Technology (KAIST)
Daejeon 34141, Republic of Korea

The ORCID identification number(s) for the author(s) of this article can be found under https://doi.org/10.1002/smll.202307542

DOI: 10.1002/smll.202307542

Although not much research has been done, several strategies have been proposed for developing stretchable batteries.[9,10] For structural stretchability, a method of pre-straining a stretchable substrate, attaching anode/cathode materials with or without current collectors, and releasing tension to form a wrinkled structure were developed.[11–13] The stretchable electrode with a 3D microporous PDMS template,[14,15] fibrous,[16–18] and serpentine structures[19,20] were also suggested. As a method of imparting elasticity to the material, stretchable electrodes were fabricated by compositing with elastomers and electrode materials.[21–23] However, most of the suggested approaches have a disadvantage in that performance is significantly degraded by introducing a significant amount of elastomer irrelevant to energy storage only for stretchability. Furthermore, most of the suggested energy storage devices are not fully stretchable batteries as they impart stretchability to specific components, while others lean on the stretchable component's stretchability.[21,24]

Our research group recently fabricated stretchable lithium-ion battery anode and cathode with inwardly protruded reentrant micro-honeycomb structures using only inorganic active material particles with graphene and CNTs without any elastomer.[25] Reentrant structures can impart structural stretchability even to non-stretchable materials because the inwardly bent network expands outward during stretching.[26–29] In addition, combined with a gel electrolyte, we created a stretchable full-cell lithium-ion battery that does not degrade energy storage performance even when it is stretchable, compared to conventional batteries. The stretchable lithium-ion battery full cell using stretchable lithium-ion conducting polymers as a material that imparts elasticity to all components[30,31] was also developed recently. However, these studies have the disadvantage of generating a low voltage of 1.7 V using only lithium metal oxide-based anode particles such as lithium titanium oxide (LTO) because of the ease of processing and stable operation. They only focused on the stretchable full batteries, there is a lack of consideration for high energy storage density in a small volume, which is the most essential in wearable energy storage systems.

Among the lithium-ion batteries (LIBs), lithium metal batteries are one of the most promising candidates for next-generation batteries.[6,32] The lithium metal anode has a 10 times higher theoretical specific capacity (3860 mAh g^{-1}) than typical graphite-based anode in lithium-ion batteries. In addition, lithium metal possesses the lowest negative electrochemical potential (−3.04 V vs the standard hydrogen electrode).[33,34] Thus, the lithium metal battery can achieve much higher capacity and higher voltage window than general lithium-ion batteries, which can have higher energy density in the same volume. However, despite these great advantages, it is very difficult to utilize lithium metal directly due to the infinite volume change and dendrites growth on the lithium metal surface during charging and discharging,[35] although much research is in progress.[36–38] Furthermore, providing stretchability to the lithium metal electrode is very difficult due to the lack of elasticity and low yield/tensile strength of lithium metal itself, thus only one study showed a stretchable lithium metal electrode based on lithium electroplated on coiled copper and embedded in an elastomer.[39]

In this study, we present a stretchable lithium metal electrode using an inwardly protruded reentrant structure of conductive graphene and CNT nano-networks with a small amount of lithiophilic MXene as the stretchable and conductive frameworks for the electrodeposition of lithium. However, when the composite electrode is fabricated by depositing lithium on the only conductive nano-network, metallic lithium is deposited surrounding thin conductive frameworks and thus the lithium metal dominates the mechanical properties of the composite electrode, making it stiff and easily broken by tension. Here, by mimicking the interpenetrating polymer network structure, we fabricated a hierarchical interpenetrating foam structure that forms a 2D micro-honeycomb cellular structure of graphene/CNT/MXene in 3D open-cell porous melamine foam. Since the melamine foam is not conductive and lithium is not deposited on the foam, it can successfully provide stable structural deformability. After the lithium deposition process, the interpenetrated cellular composite electrodes were radially compressed to form a reentrant framework structure. At this time, the melamine foam provides structural stability during stretching through the reentrant structure, and the graphene/CNT/MXene structure is used as an efficient lithium plating framework with high conductivity, high specific surface area, and deformability. In particular, the porous and deformable structure can flexibly cope with volume expansion/contraction upon charge and discharge, and the high specific surface area of the conductive network and the presence of lithiophilic MXene can inhibit the growth of dendrites.

2. Results and Discussion

Figure 1 shows the fabrication process of the stretchable lithium metal electrode in which the micro-honeycomb graphene/CNT/MXene structures and the 3D open-cell melamine foam form a structurally stretchable reentrant framework and interpenetrating network. First, in order to enhance the elasticity of the melamine foam, the styrene-ethylene/butylene-styrene (SEBS) block copolymer, a thermoplastic rubber, was thinly coated on the struts of the circularly cut melamine foam (30 mm diameter, 1 mm thick) by immersing in the SEBS solution (1 wt% in toluene) and drying by N_2 blowing. Figure S1 (Supporting Information) shows the SEBS mainly coated the melamine struts and some SEBS thin membranes at the holes were observed. Then, a 3.5:5:1.5 weight ratio of graphene oxide (GO), well-dispersed single-walled CNTs, and few-layer MXene nanoplatelet were mixed well in an aqueous medium, and the SEBS-coated melamine foam was immersed in the solution for soaking then placed on the copper foil, and a directional freezing self-assembly method[25,26] was performed with liquid nitrogen. As a result, the sparse (less than 1% of volume) melamine foam structure did not affect the temperature gradient from the bottom liquid nitrogen, so micro-sized ice pillars grew in the direction of the vertical temperature gradient. Then, vertically aligned 2D GO/CNT/MXene micro-honeycomb structures within the melamine foam were obtained through the sublimation of ice crystals. Then, the GO/CNT/MXene in melamine foam (MF) was reduced with hydrazine vapor at 80 °C overnight to obtain graphene/CNT/MXene-MF (GCMMF). Lithium was then electrodeposited onto the interpenetrated GCMMF network at 0.75 mA from lithium foil in a beaker cell with 1 M LiTFSI electrolyte of DME:DOL (1:1 vol%) with 2 wt% $LiNO_3$. Naturally, as lithium is deposited, the electrode framework becomes thicker, limiting the flexibility of the anode.

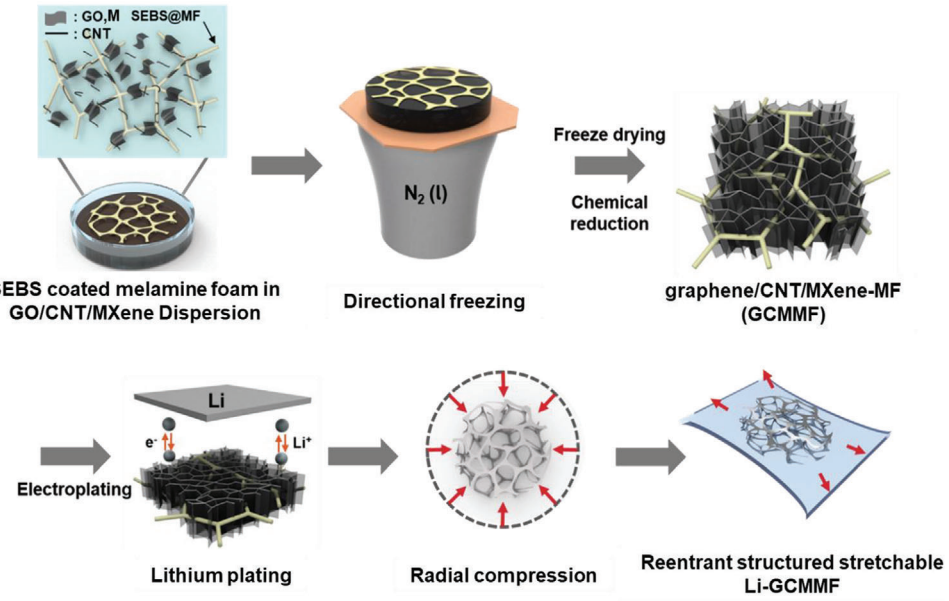

Figure 1. Schematic illustration of the Li–graphene/CNT/MXene-MF (Li-GCMMF) electrode fabrication. Hierarchically interpenetrating reentrant structures of 2D cellular graphene/CNT/MXene networks and 3D open-cell melamine foam can be fabricated by sequential directional freezing, electroplating, and radial compression. Therefore, stretchable lithium metal electrodes can be implemented in a form in which independent lithium plating occurs only on the electrical skeleton, while the melamine foam is responsible for stretchability.

However, the deformable properties can be maintained due to the interpenetrating structure with the 3D cellular melamine foam. The Li-electroplated GCMMF network then formed a reentrant structure through radial compression from 25 to 16 mm in diameter.

The microscopic morphologies of the hierarchically interpenetrated microcellular structure of the GCMMF structures with aligned pores through directional freezing are shown in **Figure 2**. The framework of the honeycomb-shaped cellular structure consists of 2D graphene nanosheets, 1D CNTs nanofiber and smaller

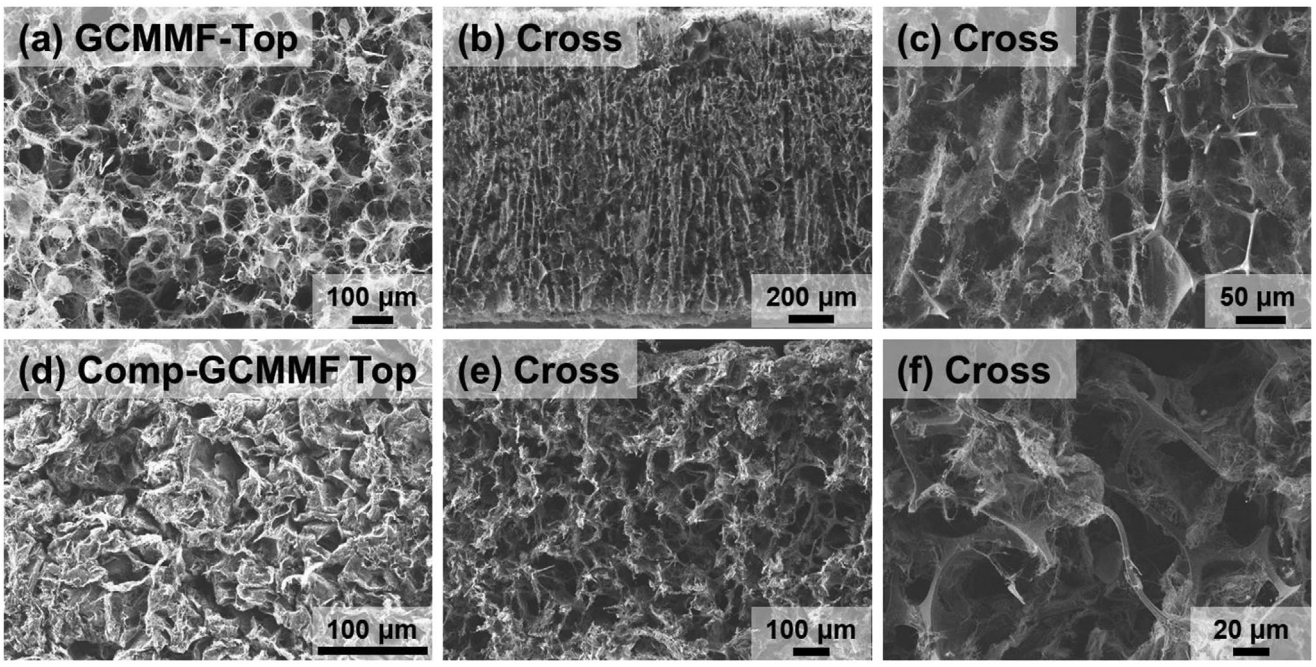

Figure 2. a,d) Top surface and b,c,e,f) cross-sectional SEM images of the GCMMF frameworks formed by directional freezing of graphene/CNT/MXene suspensions in a 3D open-cell melamine foam a–c) before and d–f) after the radial compression.

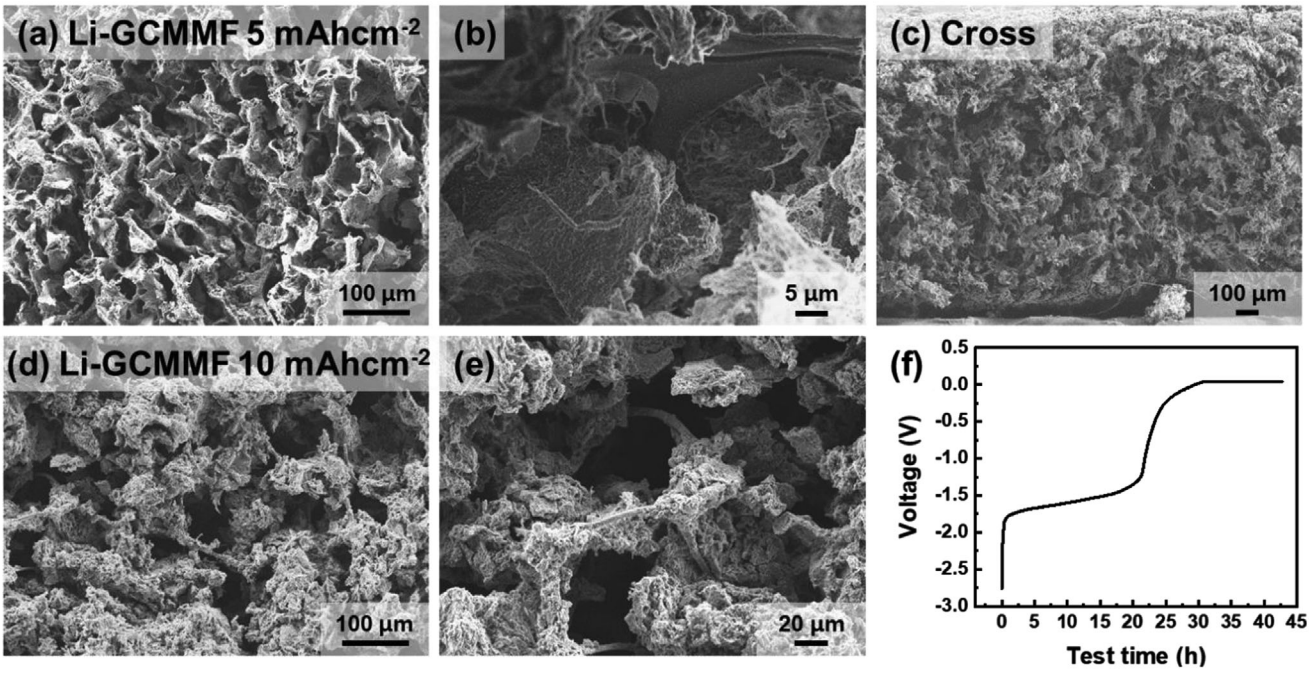

Figure 3. a–e) SEM images of reentrant lithium-plated Li-GCMMF frameworks after radial compression process with electrodeposition of lithium a–c) at 5 mAh cm^{-2} and d,e) at 10 mAh cm^{-2}. f) Voltage–time plot of electroplating at 5 mAh cm^{-2} to the GCMMF electrodes.

nanoplates of MXene, and their pore size ranges from 10 to 30 µm. Through the EDS analysis images in Figure S2 (Supporting Information), it can be observed that the elements C, O, Ti, N, and F corresponding to GO, CNT, and MXene are uniformly distributed to form a structure. In the framework formed by mixing GO, CNT, and MXene in a ratio of 3.5:1.5:5, carbon corresponding to CNT and graphene is most abundant at 71.42 wt%, while titanium from MXene is 12.60 wt%. Additionally, the elements oxygen, nitrogen, and fluorine corresponding to the functional groups of graphene and MXene are 12.28 wt%, 1.89 wt%, and 1.81 wt%, respectively. The conductive networks formed by GO, CNT, and MXene are well dispersed without agglomeration, maintaining uniform lithium deposition and mechanical stability. The relatively larger melamine foam structure was rarely observed on the top surfaces (Figure 2a) and bottom (Figure 2b). However, in the cross-section of Figure 2c, it was observed that the 3D open-cell structure melamine foam with approximately 70–100 µm pores was interpenetrated between the vertically aligned graphene/CNT/MXene framework throughout the thickness. If two different cellular structures interpenetrate within one structure, the graphene/CNT/MXene can serve as a framework for the electrodeposition of lithium metal, and melamine foam can serve as a sponge to cope with mechanical deformation, thus achieving two properties at the same time. After the radial compression with 50% areal compression, the GCMMF without the lithium deposition (Figure 2d) showed higher density and inwardly protruded graphene/CNT/MXene cellular frameworks and, at the same time, many inwardly bent struts of the melamine foam are observed. In particular, in the higher magnification SEM image of Figure 2e, despite the interpenetrating structure between the two, it was observed that the inwardly protruded melamine struts existed independently and smoothly without graphene/CNT/MXene coating, confirming that they could have stable stretchability even after subsequent lithium deposition.

After the deposition of various amounts of lithium and subsequent radial compression, the microscopic morphologies of the reentrant GCMMF structures can be seen in **Figure 3**. Figure 3a–c shows the GCMMF structure after lithium deposition at 5 mAh cm^{-2} and subsequent radial compression. Lithium plating was performed through electroplating at a current density of 0.75 mA cm^{-2}. Lithium deposition onto graphene/CNT/MXene framework in the GCMMF electrode was carried out for approximately 45 h to deposit a capacity of 5 mAh cm^{-2} (Figure 3f). During the electroplating process, lithium metal is ionized from -3 V to 0 V, and above 0 V, lithium was deposited on the GCMMF. The plateau near −1.5 V indicates an irreversible SEI is formed on the nano-carbon materials.[40] The specific surface area of the electrode is too large, so a long SEI formation proceeds, and it does not appear after 2 cycles. Through the distribution of elements after electroplating in EDS mapping in Figure S3 (Supporting Information), each element still looks uniformly distributed within the structure. Oxygen is the most abundant at 50.42 wt%, followed by fluorine at 29.13 wt%, carbon at 15.60 wt%, nitrogen at 2.69 wt%, and titanium at 2.16 wt%. Compared to Figure S2 (Supporting Information), the significant increase in oxygen and fluorine relative to the carbon and titanium ratio is expected to be due to the formation of an oxygen- and fluorine-rich SEI layer on the electrode. As shown in Figure 3a,b and Figure S4 (Supporting Information), the lithium was evenly plated on the graphene/CNT/MXene framework, and the lithium-plated framework also formed an inwardly curved cellular structure. In addition, the melamine

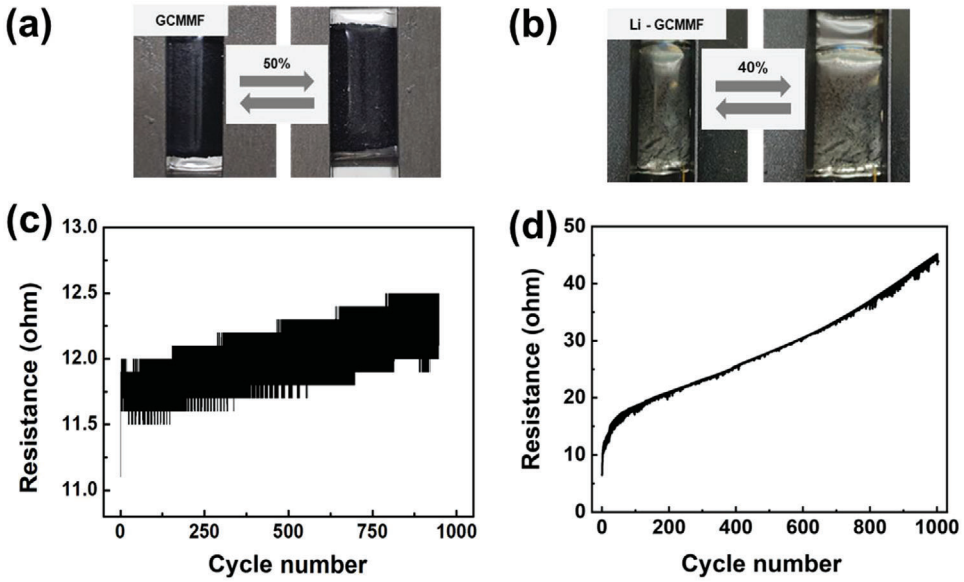

Figure 4. Photograph images showing a) the reentrant pristine GCMMF electrode and b) 5 mAh cm^{-2} of lithium deposited reentrant Li-GCMMF electrode at unstrained and strained states. c,d) Resistance changes of c) the GCMMF electrode under the repetitive stretching/releasing cycles at 50% strain up to 1000 cycles. d) 5 mAh cm^{-2} of Li-GCMMF electrode under the repetitive stretching/releasing cycles at 40% strain up to 1000 cycles.

struts maintained a smooth surface without any adhered materials after the lithium deposition process, allowing the structure to stably maintain against mechanical deformation regardless of the deposition. The vertically aligned structure of Li-GCMMF is also stably maintained after the Li deposition, as shown in the cross-section SEM image of Figure 3c. Even when the lithium deposition was increased to 10 mAh cm^{-2} (Figure 3d,e), the lithium-deposited conductive frameworks were thickened and showed a slightly mossy morphology, but still maintained the reentrant morphology, and the melamine foam struts still existed skinny and inwardly bent regardless of the lithium deposition. So, they can simultaneously maintain the stretch characteristics and works as lithium metal electrode.

Next, as shown in **Figure 4**, the GCMMF electrodes subjected to radial compression with and without lithium deposition at 5 mAh cm^{-2} were sandwiched in VHB encapsulant film and clamped into a jig (Figure 4a,b), and the resistance change was measured in repeated stretch/release tests. The resistance ratio of the radially compressed pristine (no lithium) GCMMF electrodes (Figure 4a,c) between the tensioned and released states barely changed by ≈1.04, because, as shown in our previous papers,[25,26] the reentrant structure of conductive graphene/CNT/MXene framework is highly stable to tensile deformation. Moreover, even after 1000 repetitions of the tensioned/released test, the change in resistance (R/R_0) was barely changed by less than 1.05. These stable conduction properties against mechanical deformation indicate that this interpenetrating reentrant structure is ideal for stretchable electrodes. The structure maintains stable mechanical integrity under stretched states even after being wetted with electrolyte. Even in the case of the lithium-deposited compressed Li-GCMMF electrode, only a relatively low resistance change of less than 1.2 was observed in the 40% stretch/release test, although higher than the pristine (lithium-free) GCMMF electrode. In addition, as a result of repeating 40% of stretch/release experiments up to 1000 cycles in Figure 4d, it was confirmed that although resistance increased steadily, large-scale cracks were not observed, and low resistance was maintained. However, the radially compressed cellular GCM structure without melamine foam could not withstand 40% elongation and was torn due to the deposition of lithium on the framework itself (Figure S5, Supporting Information). This result indicates that although metallic lithium is deposited on the conductive framework, increasing the stiffness and decreasing the flexibility, the reentrant and interpenetrated melamine struts can take up most of the mechanical deformation and maintain its elasticity. We conducted tensile tests of the GCMMF and Li-GCMMF electrodes until fracture occurred and measured the change in resistance until fracture in Figure S6 (Supporting Information). In the case of GCMMF without lithium, the electrode could be stretched up to 300% without significant change in resistance, and fracture occurred at 310%. Lithium-deposited Li-GCMMF electrode could be stretched up to 100% without significant change in resistance, and fracture occurred at 100%.

To investigate the electrochemical performance of the fabricated Li-GCMMF electrode, electrochemical impedance spectroscopy (EIS) and Li cell tests were conducted, comparing them with bare lithium foil and Li-graphene/CNT-MF (Li-GCMF) without MXene nanoplates. As shown in **Figure 5**a, by analyzing the EIS for each electrode with lithium foil as a counter electrode,[41] the bulk resistance (R_{bulk}) and the charge transfer resistance (R_{ct}) related to the resistance of the interface in the SEI (Solid Electrolyte Interphase) layer were obtained, respectively. The R_{bulk} of Li-GCMMF//Li, Li-GCMF//Li and bare Li//Li are similar values of 3.08 Ω, 2.94 Ω and 2.64 Ω, respectively. However, R_{ct}, the interfacial resistance of the electrode, shows a significantly lower resistance of 68.94 Ω for Li-GCMMF//Li compared to 91.11 Ω for Li-GCMF//Li and 216.54 Ω for bare Li//Li, indicating that the

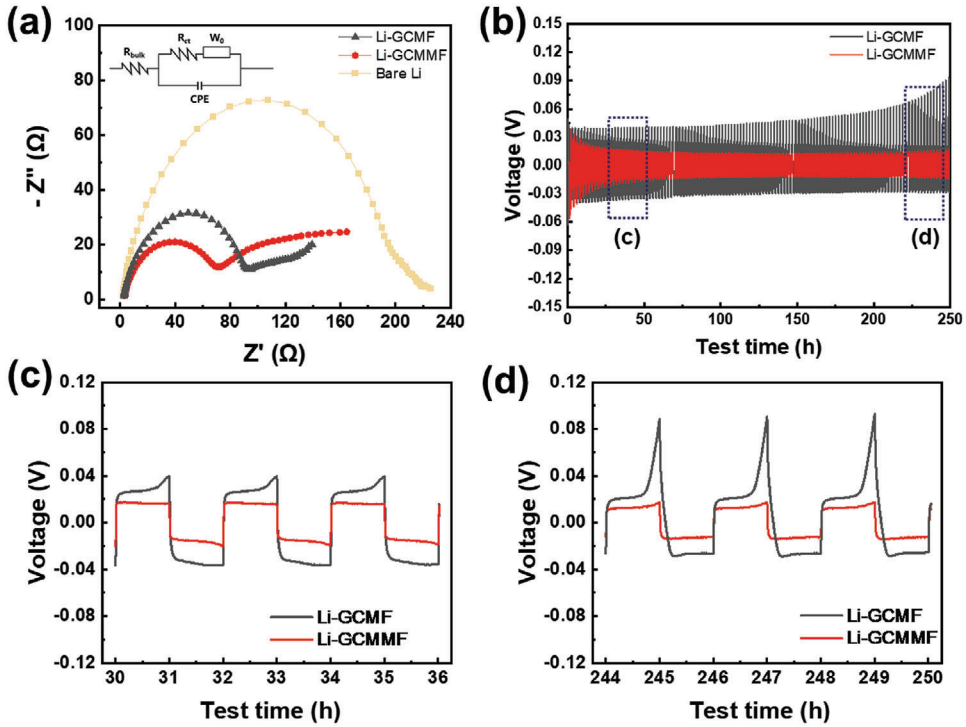

Figure 5. a) Electrochemical impedance spectra of bare Li metal foil, Li-GCMF and Li-GCMMF electrode. b) Cycling performance of Symmetric cell with Li-GCMF and Li-GCMMF at the current 0.25 mA cm^{-2} with the areal capacity of 0.25 mAh cm^{-2}. The electrolyte is 1 M LiTFSI in DME/DOL (1:1 vol%) with 2 wt% $LiNO_3$. Zoomed-in profiles of typical testing time c) 30–36 h, d) 244–250 h.

interfacial resistance of our electrodes is much smaller than that of bare lithium foil.

Furthermore, cell tests with lithium foil counter electrode were performed at a current density of 0.25 mA cm^{-2} and a capacity of 0.25 mAh cm^{-2} to assess the stability and polarization behavior during Li plating and stripping, as shown in Figure 4b–d. The Li-GCMF framework made of GO and CNT in a ratio of 5:5 without adding MXene was prepared through 5 mA cm^{-2} of Li electroplating in the same way as Li-GCMMF. The voltage profile of the Li-GCMF//Li cell initially worked well with a low overpotential of 60 mV during the stripping and plating process (Figure 3c), due to the high surface area and porous structure of the graphene and CNTs, but the overpotential gradually increased and showed sharp peaks in the latter half of stripping, as shown in Figure 4d.[42] Since the Li-GCMF electrode is made of only carbon materials and lacks lithiophilic sites, it is difficult to perform reversible charging and discharging, and thus dead lithium are gradually generated in the Li-GCMF electrode, resulting in a gradual decrease in performance. On the other hand, in the Li-GCMMF//Li cell, the voltage polarization was not large from the reversible movement of lithium due to the presence of MXene with high lithiophilicity. Although the Li-GCMMF showed a relatively high overpotential in the initial cycle due to the formation of a new SEI layer over a much higher surface area, after that, a stable SEI layer from the MXene was formed, and reversible lithium charging and discharging became possible. As a result, the Li-GCMMF//Li cell exhibited a stable performance with overpotentials as low as about 20 mV and over 125 charge/discharge cycles (Figure 5b). The negatively charged surface groups found in MXene, such as —F, —O, and —OH, serve as lithiophilic sites that help uniform lithium deposition and promote the formation of a stable solid electrolyte interface (SEI),[43] resulting in stable performance.

To fabricate a stretchable lithium metal battery full cell, we follow the strategies used in our previous study for intrinsically stretchable and printable lithium-ion batteries.[31] We introduced OH functional groups into PVDF to enhance interfacial adhesion with active materials and induced physical crosslinking for stable elasticity. Stretchable cathodes were fabricated using PVDF base physically crosslinked organogels (PCOGs) as a stretchable binder, CNTs as conductive additives, and LFP particles as active cathode materials. A stretchable current collector (SCC) was fabricated using a nanocomposite of poly(styrene-*block*-isobutylene-*block*-styrene) (SIBS) matrix on multi-walled CNT and three sizes of nickel metal particle fillers. **Figure 6** shows the stretchability and electrochemical properties of the intrinsically stretchable cathode on the SCC. 1.0 M $LiPF_6$ in EC/DEC (1:1 vol%) with 7.5 wt% FEC was used as an electrolyte during the stretching/releasing and half-cell tests. The SCC showed minimal resistance changes with a rate of 5 or less up to 60% stretching, and the resistance increased slightly up to 80%, but did not break even when stretched more than 120% (Figure 6a). The PCOG-LFP stretchable cathode immersed in the electrolyte for 1 hour also showed almost no resistance change (ratio less than 2) up to 45% of stretching, but after that, a significant resistance change with the appearance of visible cracks occurred, as seen in Figure 6b. Furthermore, in half-cell tests at 1 C (Figure 6c), our stretchable PCOG-LFP on the SCC operates stably at low overpotentials of

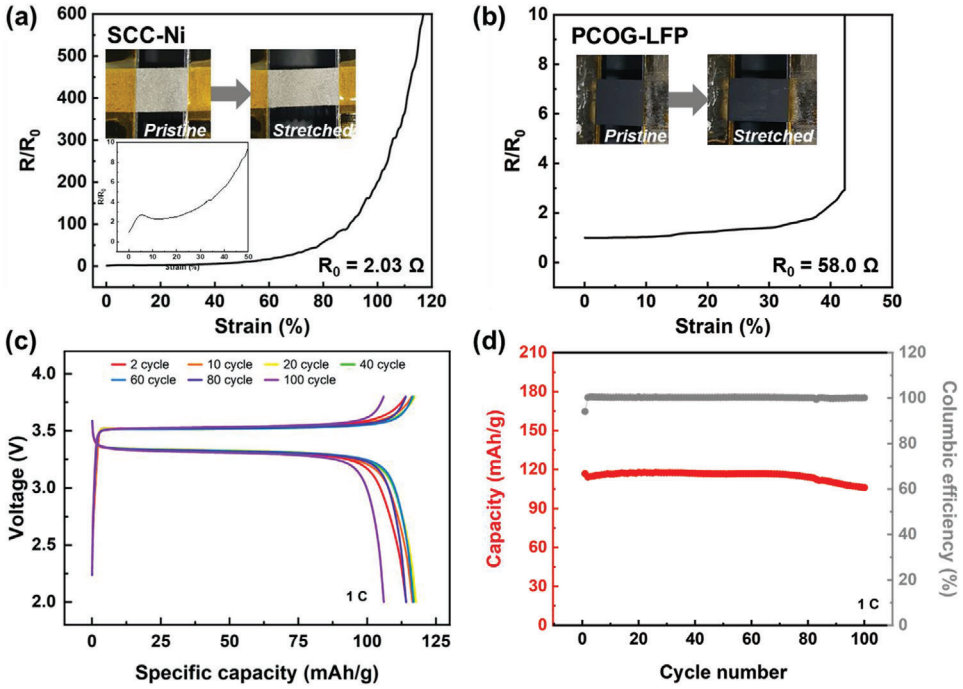

Figure 6. Resistance as a function of the strain of the a) stretchable nickel current collector (SCC-Ni), b) PCOG-LFP cathode. c) Representative charge/discharge curves of PCOG-LFP with SCC-Ni between 2.0 and 3.8 V. d) Cycling performances and coulombic efficiency of PCOG-LFP half cell at 1 C. The electrolyte is 1.0 M $LiPF_6$ in EC/DEC (1:1 vol%) with 7.5 wt% FEC.

0.17 V with a capacitance capacity and 100% of retention for 100 cycles without significant capacity loss.

Figure 7 presents a comprehensive performance and functionality of an all-stretchable lithium metal battery full cell. Before fabricating the stretchable lithium metal batteries, full cells with Li-GCMMF anode and PCOG-LFP cathode with SCC-Ni current collector were constructed in a coin cell configuration. This stretchable full cell in coin cell configuration also showed stable cycling performance of 134, 132, 128, 121, 118 mAh g^{-1} from 0.1, 0.2, 0.5, 0.8 C to 1 C (Figure 7a). Additionally, the full cells exhibited a low overpotential of ≈100 mV, approximately 70 mV lower than the bare lithium used in the half-cell test. This indicates that the Li-GCMMF electrode has lower resistance in the cell compared to bare lithium, enabling more stable and efficient movement of lithium ions during charge and discharge.

A schematic illustration and actual photograph of the assembled stretchable cell are provided in Figure 7b,c, highlighting the integration of a reentrant micro-honeycomb lithium metal anode, a composite-based stretchable PCOG-LFP cathode, and stretchable SCC-Ni current collector, a physically crosslinked PVDF-HFP-based stretchable separator,[31] and SIBS encapsulation.[44] The assembled components were arranged between SIBS substrates in the following order: Li-GCMMF, stretchable separator, and PCOG-LFP with SCC-Ni. Copper and nickel lead tabs were used to connect Li-GCMMF and PCOG-LFP/SCC-Ni for external connections, respectively. The charge-discharge curve of the stretchable LMB cell at unstrained state is shown in Figure S7 (Supporting Information), which demonstrates a stable profile during the precycle at 0.1 C and following cycles at 0.5 C. However, lower capacity was observed because the stretchable full cell provides poor contact between the electrode and the current collector (lead tab) and the stretchable separator still needs optimization especially for lithium metal electrodes. The fabricated stretchable LMB cell was then subjected to stretching from 0% to 30% at 10% intervals, and cycling measurements were performed for three cycles at each stretch level. Photographic images in Figure 7d show that the structure of the stretchable LMB cells remained intact even at 30% stretching without significant changes in appearance. In Figure 7e, the capacity gradually decreased as cycling progressed from the initial capacity value of 60.7 mAh g^{-1}, maintaining 70% capacity and 93% Coulombic efficiency in 12 cycles. However, it was observed that there was relatively little change in the capacity value in the 4^{th}, 7^{th}, and 10^{th} cycles, where the strain increased by 10% up to 30%. Through this, it was confirmed that the actual cell itself can have sufficient mechanical stability against an extension, twisting, or other mechanical deformations, even if the performance is deteriorated due to the lack of stability from the stretchable cell configuration.

3. Conclusion

In this study, we have developed a stretchable lithium metal electrode by incorporating a reentrant structure of conductive graphene, carbon nanotube (CNT) nano-networks, and lithiophilic MXene. Previous attempts using only the conductive nanonetwork resulted in stiff and easily broken composite electrodes. To address this, we fabricated a hierarchical interpenetrating foam structure with a 2D micro-honeycomb cellular arrangement of graphene/CNT/MXene within a 3D open-cell porous

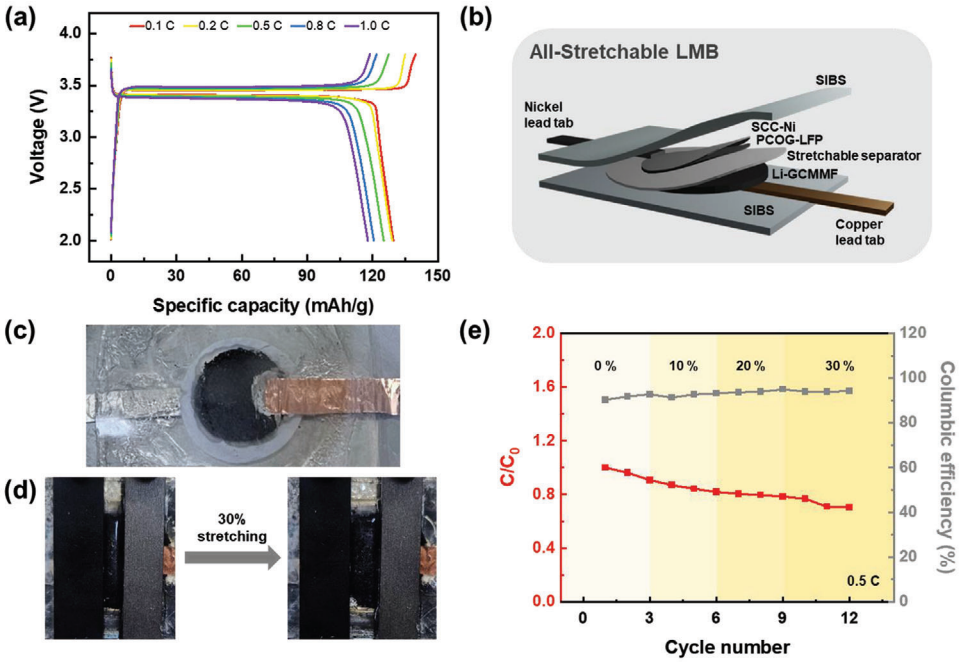

Figure 7. a) Charge/discharge curves of the Li-GCMMF and PCOG-LFP/SCC-Ni stretchable full cell in the coin cell configuration between 2.0 and 3.8 V. b) Schematic illustration and c) its actual photograph of the assembled cell of an all-stretchable battery based on the reentrant micro-honeycomb electrodes, stretchable separator, and SIBS encapsulation. d) Photographic images of the stretchable lithium metal battery at unstrained and 30% strained states. e) Discharge capacity changes and Coulombic efficiencies of the stretchable LMB with applied strain ranging from 0 to 30% at 10% intervals at 0.5 C.

melamine foam. This foam provided structural stability, while the conductive framework enabled efficient lithium plating with high conductivity and specific surface area. The electrode's porous and deformable structure accommodated volume changes during charge and discharge, and the presence of lithiophilic MXene inhibited dendrite growth. Overall, our stretchable lithium metal electrode shows promise for next-generation lithium-based energy storage devices and is expected to be widely helpful in developing all-stretchable wearable or implantable electronics as a fully stretchable energy source.

Supporting Information

Supporting Information is available from the Wiley Online Library or from the author.

Acknowledgements

Y.A. and N.K. contributed equally to this work. This work was supported by the Korea Institute of Science and Technology (KIST) Institutional Program and KU-KIST program (Project No. 2E32501, 2E32503 and 2V09840-23-P025), and the National Research Foundation of Korea (NRF) grant funded by the Korean government (No. NRF-2022R1A2B5B02001597 and 2022R1A5A1032539).

Conflict of Interest

The authors declare no conflict of interest.

Data Availability Statement

The data that support the findings of this study are available from the corresponding author upon reasonable request.

Keywords

graphene/CNT/MXene composite, hierarchically interpenetrated microcellular framework, reentrant framework, stretchable battery, stretchable lithium metal battery

Received: August 29, 2023
Revised: October 23, 2023
Published online:

[1] S. Gong, W. Cheng, *Adv. Energy Mater.* **2017**, *7*, 1700648.
[2] S. Xu, Y. Zhang, L. Jia, K. E. Mathewson, K.-I. Jang, J. Kim, H. Fu, X. Huang, P. Chava, R. Wang, S. Bhole, L. Wang, Y. J. Na, Y. Guan, M. Flavin, Z. Han, Y. Huang, J. A. Rogers, *Science* **2014**, *344*, 70.
[3] D. Son, J. Lee, S. Qiao, R. Ghaffari, J. Kim, J. E. Lee, C. Song, S. J. Kim, D. J. Lee, S. W. Jun, S. Yang, M. Park, J. Shin, K. Do, M. Lee, K. Kang, C. S. Hwang, N. Lu, T. Hyeon, D.-H. Kim, *Nat. Nanotechnol.* **2014**, *9*, 397.
[4] M. Stoppa, A. Chiolerio, *Sensors* **2014**, *14*, 11957.
[5] K. Guk, G. Han, J. Lim, K. Jeong, T. Kang, E.-K. Lim, J. Jung, *Nanomaterials* **2019**, *9*, 813.
[6] X.-B. Cheng, R. Zhang, C.-Z. Zhao, Q. Zhang, *Chem. Rev.* **2017**, *117*, 10403.
[7] X. Wang, Z. Pan, J. Yang, Z. Lyu, Y. Zhong, G. Zhou, Y. Qiu, Y. Zhang, J. Wang, W. Li, *Energy Storage Mater.* **2019**, *22*, 179.

[8] K. Liu, B. Kong, W. Liu, Y. Sun, M.-S. Song, J. Chen, Y. Liu, D. Lin, A. Pei, Y. Cui, *Joule* **2018**, *2*, 1857.
[9] W. Liu, M.-S. Song, B. Kong, Y. Cui, *Adv. Mater.* **2017**, *29*, 1603436.
[10] X. Gong, Q. Yang, C. Zhi, P. S. Lee, *Adv. Energy Mater.* **2021**, *11*, 2003308.
[11] W. Weng, Q. Sun, Y. Zhang, S. He, Q. Wu, J. Deng, X. Fang, G. Guan, J. Ren, H. Peng, *Adv. Mater.* **2015**, *27*, 1363.
[12] C. Shi, T. Wang, X. Liao, B. Qie, P. Yang, M. Chen, X. Wang, A. Srinivasan, Q. Cheng, Q. Ye, A. C. Li, X. Chen, Y. Yang, *Energy Storage Mater.* **2019**, *17*, 136.
[13] W. Liu, J. Chen, Z. Chen, K. Liu, G. Zhou, Y. Sun, M.-S. Song, Z. Bao, Y. Cui, *Adv. Energy Mater.* **2017**, *7*, 1701076.
[14] W. Liu, Z. Chen, G. Zhou, Y. Sun, H. R. Lee, C. Liu, H. Yao, Z. Bao, Y. Cui, *Adv. Mater.* **2016**, *28*, 3578.
[15] H. Li, Y. Ding, H. Ha, Y. Shi, L. Peng, X. Zhang, C. J. Ellison, G. Yu, *Adv. Mater.* **2017**, *29*, 1700898.
[16] Y. Zhang, W. Bai, X. Cheng, J. Ren, W. Weng, P. Chen, X. Fang, Z. Zhang, H. Peng, *Angew. Chem., Int. Ed.* **2014**, *53*, 14564.
[17] A. M. Zamarayeva, A. E. Ostfeld, M. Wang, J. K. Duey, I. Deckman, B. P. Lechêne, G. Davies, D. A. Steingart, A. C. Arias, *Sci. Adv.* **2017**, *3*, e1602051.
[18] Y. Sun, R. B. Sills, X. Hu, Z. W. Seh, X. Xiao, H. Xu, W. Luo, H. Jin, Y. Xin, T. Li, Z. Zhang, J. Zhou, W. Cai, Y. Huang, Y. Cui, *Nano Lett.* **2015**, *15*, 3899.
[19] S. Xu, Y. Zhang, J. Cho, J. Lee, X. Huang, L. Jia, J. A. Fan, Y. Su, J. Su, H. Zhang, H. Cheng, B. Lu, C. Yu, C. Chuang, T.-I. Kim, T. Song, K. Shigeta, S. Kang, C. Dagdeviren, I. Petrov, P. V. Braun, Y. Huang, U. Paik, J. A. Rogers, *Nat. Commun.* **2013**, *4*, 1543.
[20] J. W. Lee, R. Xu, S. Lee, K.-I. Jang, Y. Yang, A. Banks, K. J. Yu, J. Kim, S. Xu, S. Ma, S. W. Jang, P. Won, Y. Li, B. H. Kim, J. Y. Choe, S. Huh, Y. H. Kwon, Y. Huang, U. Paik, J. A. Rogers, *Proc. Natl. Acad. Sci. USA* **2016**, *113*, 6131.
[21] W.-J. Song, J. Park, D. H. Kim, S. Bae, M.-J. Kwak, M. Shin, S. Kim, S. Choi, J.-H. Jang, T. J. Shin, S. Y. Kim, K. Seo, S. Park, *Adv. Energy Mater.* **2018**, *8*, 1702478.
[22] M. Gu, W.-J. Song, J. Hong, S. Y. Kim, T. J. Shin, N. A. Kotov, S. Park, B.-S. Kim, *Sci. Adv.* **2019**, *5*, eaaw1879.
[23] S. Choi, T.-W. Kwon, A. Coskun, J. W. Choi, *Science* **2017**, *357*, 279.
[24] X. Chen, H. Huang, L. Pan, T. Liu, M. Niederberger, *Adv. Mater.* **2019**, *31*, 1904648.
[25] S. Kang, S. Y. Hong, N. Kim, J. Oh, M. Park, K. Y. Chung, S.-S. Lee, J. Lee, J. G. Son, *ACS Nano* **2020**, *14*, 3660.
[26] B. S. Kim, K. Lee, S. Kang, S. Lee, J. B. Pyo, I. S. Choi, K. Char, J. H. Park, S.-S. Lee, J. Lee, J. G. Son, *Nanoscale* **2017**, *9*, 13272.
[27] N. Variability, A. Physcss, W. Meteorolgica, O. Symposium, R. Lakes, *Science* **1987**, *235*, 1038.
[28] G. N. Greaves, A. L. Greer, R. S. Lakes, T. Rouxel, *Nat. Mater.* **2011**, *10*, 823.
[29] K. Bertoldi, P. M. Reis, S. Willshaw, T. Mullin, *Adv. Mater.* **2010**, *22*, 361.
[30] W. Liu, J. Chen, Z. Chen, K. Liu, G. Zhou, Y. Sun, M. S. Song, Z. Bao, Y. Cui, *Adv. Energy Mater.* **2017**, *7*, 1701076.
[31] S. Y. Hong, S. M. Jee, Y. Ko, J. Cho, K. H. Lee, B. Yeom, H. Kim, J. G. Son, *ACS Nano* **2022**, *16*, 2271.
[32] M. J. Lee, J. Han, K. Lee, Y. J. Lee, B. G. Kim, K.-N. Jung, B. J. Kim, S. W. Lee, *Nature* **2022**, *601*, 217.
[33] W. Xu, J. Wang, F. Ding, X. Chen, E. Nasybulin, Y. Zhang, J.-G. Zhang, *Energy Environ. Sci.* **2014**, *7*, 513.
[34] D. Lin, Y. Liu, Y. Cui, *Nat. Nanotechnol.* **2017**, *12*, 194.
[35] M. D. Tikekar, S. Choudhury, Z. Tu, L. A. Archer, *Nat. Energy* **2016**, *1*, 16114.
[36] P. Zhao, Y. Li, S. Chen, H. Fan, Y. Feng, L. Hu, Y. Zhang, Q. Nie, H. Pei, C. Yang, J. Deng, C. Bao, J. Song, *Adv. Energy Mater.* **2022**, *12*, 2200568.
[37] Y. Zhang, P. Zhao, Q. Nie, Y. Li, R. Guo, Y. Hong, J. Deng, J. Song, J. Song, *Adv. Mater.* **2023**, *35*, 2211032.
[38] A. Wang, J. Li, M. Yi, Y. Xie, S. Chang, H. Shi, L. Zhang, M. Bai, Y. Zhou, Y. Lai, Z. Zhang, *Energy Storage Mater.* **2022**, *49*, 246.
[39] Y. Yu, Y. Zhu, X. Zhang, *Joule* **2018**, *2*, 1654.
[40] G. Yang, Y. Li, Y. Tong, J. Qiu, S. Liu, S. Zhang, Z. Guan, B. Xu, Z. Wang, L. Chen, *Nano Lett.* **2019**, *19*, 494.
[41] P. Gao, C. Zhang, G. Wen, *J. Power Sources* **2015**, *294*, 67.
[42] K.-H. Chen, K. N. Wood, E. Kazyak, W. S. Lepage, A. L. Davis, A. J. Sanchez, N. P. Dasgupta, *J. Mater. Chem. A* **2017**, *5*, 11671.
[43] H. Shi, C. J. Zhang, P. Lu, Y. Dong, P. Wen, Z.-S. Wu, *ACS Nano* **2019**, *13*, 14308.
[44] T. N. Nguyen, B. Iranpour, E. Cheng, J. D. W. Madden, *Adv. Energy Mater.* **2021**, *12*, 2103148.